Structure, Vol. 13, 1255–1267, September, 2005, ©2005 Elsevier Ltd All rights reserved. DOI 10.1016/j.str.2005.05.015

Structure and Dynamics of an RNA Tetraloop: A Joint Molecular Dynamics and NMR Study

Jessica Koplin,[1] Yuguang Mu,[1,3] Christian Richter,[2] Harald Schwalbe,[2] and Gerhard Stock[1,*]
[1]Institute of Physical and Theoretical Chemistry
[2]Institute for Organic Chemistry and Chemical Biology
Center for Biomolecular Magnetic Resonance
Johann Wolfgang Goethe-University, Frankfurt
Marie-Curie-Str 11
D-60439 Frankfurt/Main
Germany

Summary

Molecular dynamics simulations of the RNA tetraloop 5′-CGCUUUUGCG-3′ with high melting temperature and significant conformational heterogeneity in explicit water solvent are presented and compared to NMR studies. The NMR data allow for a detailed test of the theoretical model, including the quality of the force field and the conformational sampling. Due to the conformational heterogeneity of the tetraloop, high temperature (350 K) and locally enhanced sampling simulations need to be invoked. The Amber98 force field leads to a good overall agreement with experimental data. Based on NMR data and a principal component analysis of the 350 K trajectory, the dynamic structure of the tetraloop is revealed. The principal component free energy surface exhibits four minima, which correspond to well-defined conformational structures that differ mainly by their base stacking in the loop region. No correlation between the motion of the sugar rings and the stacking dynamics of the loop bases is found.

Introduction

The hairpin motif is a ubiquitous structural motif of RNA and DNA oligonucleotides (Woese et al., 1990). RNA hairpins emerge when the single-stranded RNA molecule folds back on itself to form a double-helical stem capped by a loop of unpaired nucleotides. They play important roles in both RNA structure and function, e.g., hairpins are thought to provide nucleation sites for RNA folding (Uhlenbeck, 1990) and tertiary recognition sites for both proteins and nucleic acids (Jagath et al., 2001; Legault et al., 1998). In particular, tetraloops (RNA hairpins with four nucleotides) are commonplace and have therefore been the focus of recent structural investigations, including nuclear magnetic resonance (NMR) (Butcher et al., 1997; Cheong et al., 1990; Du et al., 2003; Furtig et al., 2004; Heus and Pardi, 1991; Jucker and Pardi, 1995; Jucker et al., 1996) and molecular dynamics (MD) studies (Cheatham, 2004; Kajava and Ruterjans, 1993; Miller and Kollman, 1997; Sorin et al., 2002, 2003; Williams and Hall, 1999, 2000a, 2000b; Zacharias, 2000). The focus of these studies has been the investigation of stable tetraloops, especially of UNCG, GNRA, and CUUG loops, which represent the most frequently occurring hairpins both in prokaryotic and eukaryotic RNAs. The stability of these classes of tetraloops has been attributed to the additional base pairs formed between nucleotides 1 and 4 in the loop, back stacking, and several 2′ OH-base hydrogen bonds (Sorin et al., 2002; Williams and Hall, 2000a).

However, other sequences can also form hairpin structures, and their melting temperatures have been determined (Antao et al., 1991; Proctor et al., 2002, 2004): for example, the sequence of four repetitive uridine nucleotides, flanked by a short, three base pairs-containing stem, forms a stable hairpin with melting temperatures for the sequences gUUUUc and cUUUUg of 51.5° and 60.4°C, respectively. The melting temperatures are therefore only 8.6°C and 11.3°C decreased compared to the most stable 12mer hairpins gUUCGc and cUUCGg, respectively (Antao et al., 1991). The decrease is, however, more pronounced for 10mer hairpins (cUUCGg: 72.6°C compared to cUUUUg: 56.8°C) (Wörner, 1997).

From all diribonucleotides, the stacking interaction of the UpU dinucleotide has been reported to be the weakest (Norberg and Nilsson, 1995). Hairpins containing the UUUU tetraloop have been incorporated as flanking loops for RNA quadruplexes (Liu et al., 2002) and have been investigated in the context of the functional anticodon architecture of $tRNA^{Lys3}$ (Durant and Davis, 1999; Stuart et al., 2000). In addition, the incorporation of a UUUU tetraloop in loop II of the hammerhead ribozyme leads to a 2–3 fold increase in activity compared to the more stable GCAA tetraloop in this position (Eckstein et al., 2001; Persson et al., 2002). The findings are furthermore supported by data from Conaty et al. (1999) showing that loops of polypyrimidines rather than very stable tetraloop structures are important for efficient cleavage activity of the hammerhead ribozyme.

The structure determination of this class of flexible tetraloops is more difficult than for stable tetraloops, since NMR data are averaged over the ensemble of conformers. Recently, Schwalbe and coworkers have reported extensive NMR studies on the RNA tetraloop 5′-CGCUUUUGCG-3′, including NOEs, various ^{3}J couplings, and crosscorrelated relaxation rates (Duchardt et al., 2001; Felli et al., 1999; Richter et al., 1998, 2000). Using these methods, it has been shown that the loop nucleotide U6 of the UUUU tetraloop is conformationally averaged between the N- and the S-type sugar pucker mode (Duchardt et al., 2001), thus indicating significant conformational dynamics. Representing a structural description of a small RNA loop in great detail, these NMR results may serve as benchmark data to study the validity and accuracy of an MD description of RNA systems (Auffinger et al., 2003; Auffinger and Westhof, 2000; Beveridge and McConnell, 2000; Gouda et al., 2003; Norberg and Nilsson, 2002; Tsui and Case, 2001; Zacharias and Sklenar, 1999). The purpose of the

*Correspondence: stock@theochem.uni-frankfurt.de
[3]Present address: School of Biological Science, Nanyang Technology University, Nanyang Drive 60, Singapore 637551.

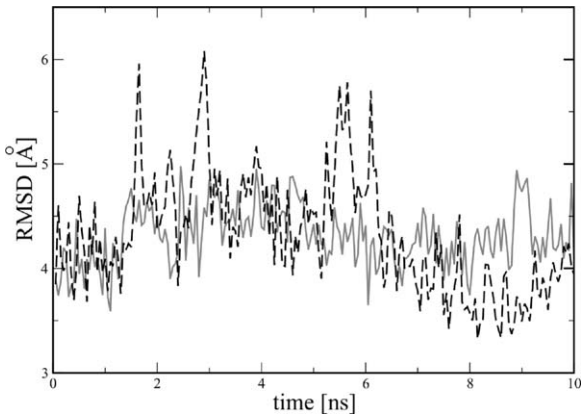

Figure 1. Time Evolution of the Rmsd Obtained for Trajectories MD1 at 300 K and for the 350 K Simulation

The trajectories MD1 at 300 K are shown by a solid line, and the 350 K simulation is shown by a dashed line.

current work is therefore two fold. First, by comparing experimental and theoretical data, we studied the quality and performance of the theoretical model, including the force field, the conformational sampling, and the modeling of NMR data via approximate formulae such as Karplus relations. Second, combining the results of NMR and simulation, a picture of the dynamic structure of the UUUU tetraloop is developed that could not be obtained by conventional NMR-derived structures.

Results

General Characterization of MD Runs

As a first check of quality, we have considered the root mean square distance (rmsd) of all trajectories with respect to their initial NMR starting structure. As a representative example, Figure 1 shows the time evolution of the rmsd of trajectory MD1 at 300 K. The rmsd is seen to fluctuate around 4.5 Å for times $>\sim 2$ ns, thus reflecting a stable trajectory. Also shown is the rmsd of the high-temperature MD run at 350 K. Due to the increased temperature, the rmsd for this trajectory exhibits somewhat larger fluctuations. Nevertheless, the trajectory remains stable throughout the propagation.

To obtain an impression of the overall behavior of the various MD runs, Figure 2 shows a circle representation of the torsional angles of the four loop residues. Generally speaking, it is seen that most angles of trajectory MD1 are well described by a single mean value, thus indicating that the system predominantly stays in a single conformation. Compared to MD1, the conformational fluctuations of MD2 are significantly higher, which reflects a certain amount of conformational heterogeneity. The two trajectories at 300 K also differ in the state of the U6 sugar pucker, that is, MD1 is in C3′-endo and MD2 is in C2′-endo. Furthermore, Figure 2 shows the results obtained for the two additional trajectories with enhanced sampling, i.e., the high-temperature MD run at 350 K and the LES trajectory at 300 K. Both simulations clearly sample a larger range of coordinate space than trajectories MD1 and MD2. In particular, this is true for the backbone dihedral angles α and ζ as well as for the pseudorotation angles P, which reflect conformational transitions absent in the conventional runs MD1 and MD2.

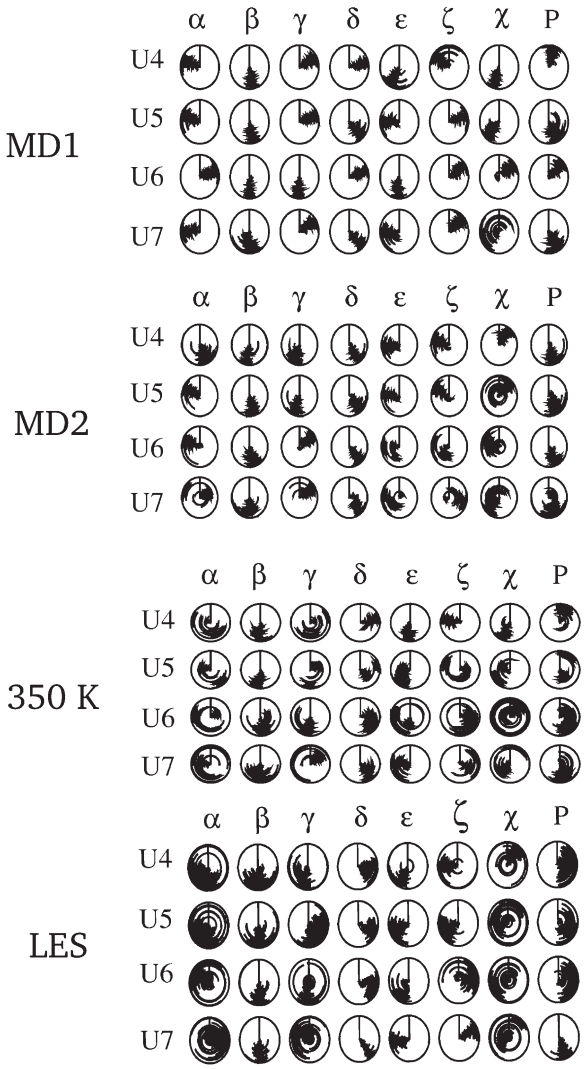

Figure 2. Circle Representation of the Torsional Angles of the UUUU Loop as Obtained from the Two Trajectories at 300 K, MD1 and MD2, as well as from the 350 K Trajectory and the LES Trajectory at 300 K

Analysis of the Experimental NMR Data

A first comparison of experimental and calculated results for the backbone angles of the UUUU loop revealed a good overall agreement for angles β, γ, and δ (see below), but significant deviations for angles α, ϵ, and ζ. In the experiment, the latter results were derived from a global fit of several ^3J couplings and crosscorrelated relaxation rates (Duchardt et al., 2001; Felli et al., 1999; Richter et al., 1998, 2000). From this fit, the results were chosen because either they were closest to the structure of the canonical form or because they had the smallest rmsd in the fit in the absence of a complete

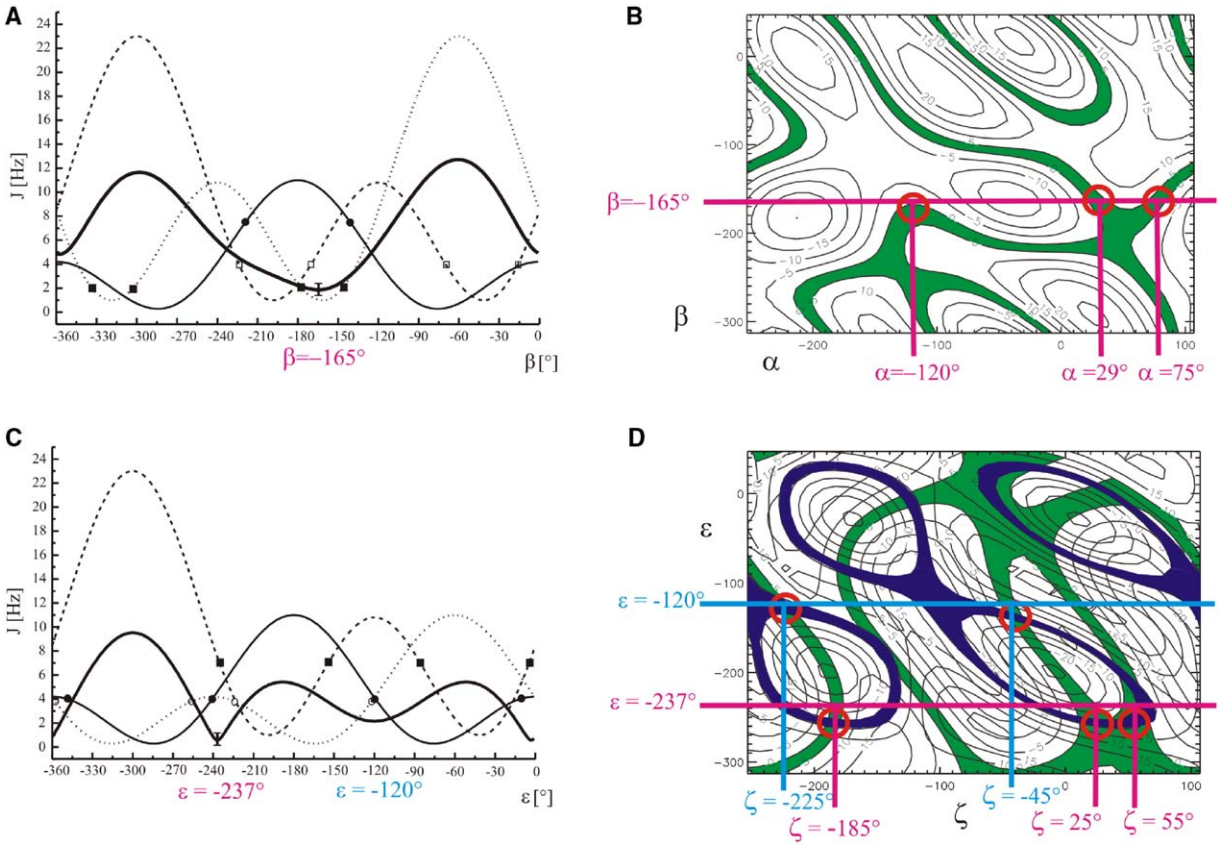

Figure 3. Determination of the Backbone Angles α, β, ϵ, and ζ from Experimental ^{3}J Couplings and CSA Crosscorrelated Relaxation Rates, Shown for the Example of the U7 Nucleotide of the UUUU Loop

The ^{3}J couplings are shown on the left, and the CSA crosscorrelated relaxation rates are shown on the right.

(A) Experimental values (as boxes) and theoretical Karplus curves (Equations 1 and 2, as lines) of various ^{3}J couplings reflecting angle β. Shown are ^{3}J(H5′$^{proS}_i$,P$_i$) drawn as an open square and a long-dashed line, ^{3}J(H5′$^{proR}_i$,P$_i$) drawn as a closed square and a short-dashed line, and ^{3}J(C4′$_i$,P$_i$) drawn as a closed circle and a solid line. Error bars have been obtained for duplicate measurements.

(B) Theoretical dependence of the CSA crosscorrelated relaxation rates $\Gamma^c_{(C5'_i,H5'_i),(P_i)} + \Gamma^c_{(C5'_i,H5''_i),(P_i)}$ on angles β and α. The red circles indicate the conformational regions that fulfill the experimental crosscorrelated relaxation rates. Assuming β = –165° as obtained in (A), possible values for angle α are –120°, 29°, and 75°.

(C) Various ^{3}J couplings reflecting angle ϵ. Shown are ^{3}J(H3′$_i$,P$_{i+1}$) drawn as a closed square and a long-dashed line, ^{3}J(C2$_i$′,P$_i$) drawn as an closed circle and a short-dashed line, and ^{3}J(C4′$_i$,P$_{i+1}$) drawn as a closed circle and a solid line.

(D) Theoretical dependence of the CSA crosscorrelated relaxation rates $\Gamma^c_{(C2'_i,H2'_i),(P_{i+1})}$ (in green) and $\Gamma^c_{(C3'_i,H3'_i),(P_{i+1})}$ (in blue) on angles ϵ and ζ. The red circles indicate the conformational regions that fulfill the experimental crosscorrelated relaxation rates. Error bars have been obtained either by duplicate measurements or from conservation error estimation.

structure calculation. Since the MD simulations provide an additional means of analyzing the experimental data, it is instructive to briefly reconsider this procedure.

Using nucleotide U7 of the UUUU loop as a representative example, Figure 3 shows various ^{3}J couplings that reflect the backbone angles β (Figure 3A) and ϵ (Figure 3C), as well as chemical-shift anisotropy/dipole-dipole (CSA-DD) crosscorrelated relaxation rates that reflect the backbone angles α, β (Figure 3B) and ϵ, ζ (Figure 3D). Comparing experimental values and Karplus curves (Equations 1 and 2) for the dihedral angle β, Figure 3A shows that β can unambiguously be obtained from the ^{3}J(H5′,^{proR},P), ^{3}J(H5′,^{proS},P) and ^{3}J(C4′,P) coupling constants; the measured couplings are consistent with a single conformation around β = –165°. To determine the angle α, the CSA-DD crosscorrelated relaxation rate from the C5′H5′ dipole onto the phosphor CSA tensor is considered. Figure 3B shows the (α,β) dependence of this rate and adopts the simple model given in Richter et al., 2000. Assuming that β = –165°, we obtain three possible values for angle α: –120°, 29°, and 75°. As α = –120° is close to the value of the canonical conformation, this result was also chosen in the interpretation of the experimental data in Richter et al. (2000).

The dihedral angle ϵ is obtained from a Karplus analysis of the coupling constants ^{3}J(H3′$_i$,P$_{i+1}$), ^{3}J(C2$_i$′,P$_i$), and ^{3}J(C4′$_i$,P$_{i+1}$) shown in Figure 3C. The fitting of the data yields two possible unambiguous solutions for angle ϵ: –120° and –237°. In the experimental analysis (Richter et al., 2000), the latter result was favored, because the rmsd obtained for ϵ = –237° is lower (±0.6°) compared to the rmsd (±2.2°) obtained for ϵ = –120°. (The reason for the lower rmsd is a value for the

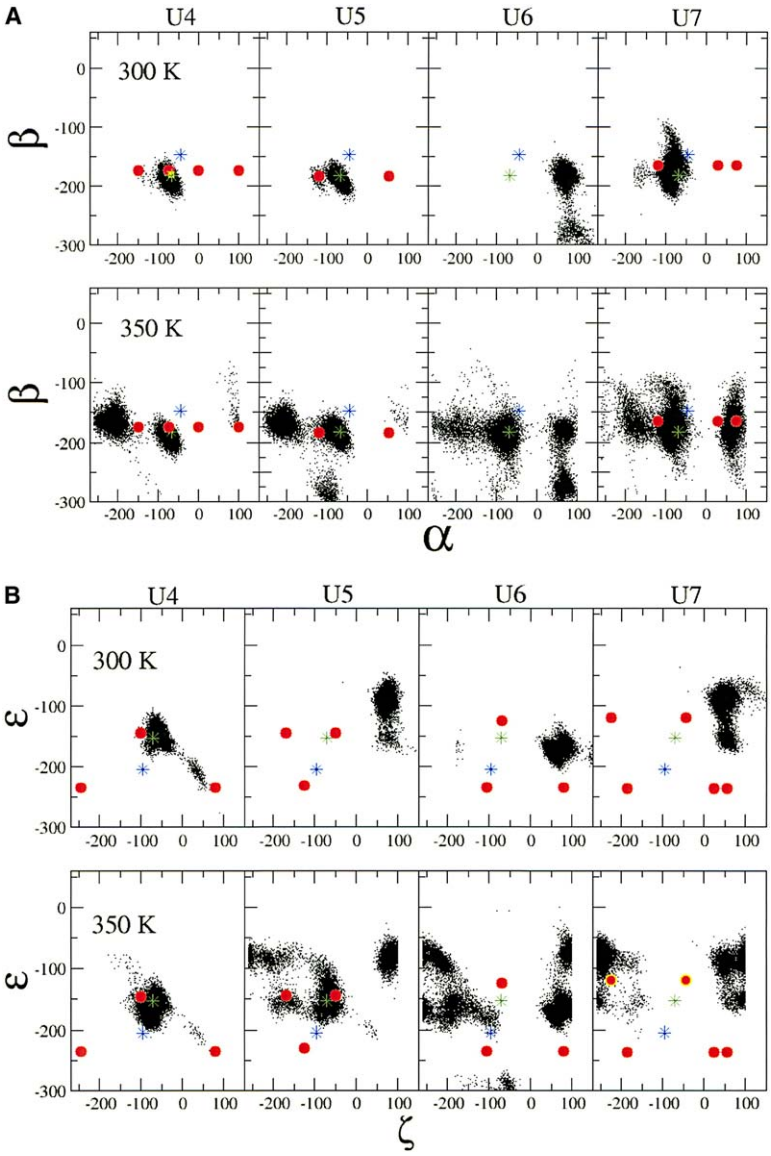

Figure 4. Joint Probability Distribution of Angles α and β and ϵ and ζ as Obtained for Trajectory MD1 at 300 K and for the 350 K Run

Angles α and β are shown in the upper panels, and ϵ and ζ are shown in the lower panels. The red dots correspond to values of the angles that are consistent with the analysis of the experimental data in Figure 3. The green and blue asterisks display the values of the canonical A and B forms, respectively.

$^3J(H3'_i,P_{i+1})$ coupling constant that is too small to be consistent with ϵ = –120°. A critical reevaluation of the applicability of the original published NMR methods to determine the $^3J(H3'_i,P_{i+1})$ coupling constant might be warranted here.) Assuming ϵ to be either –120° or –237°, the dihedral angle ζ can be extracted from the (ϵ,ζ) dependence of the corresponding CSA-DD cross-correlated relaxation rate shown in Figure 3D. We obtain ζ = –185°, 25°, or 55° for ϵ = –237°, and ζ = –225° or –45° for ϵ = –120°. In the experimental analysis (Richter et al., 2000), ζ = –185° was favored, since it is close to the value of the canonical conformation.

Comparison of MD and NMR Results

Backbone Angles

It is interesting to reconsider the analysis of above-discussed experimental data in light of the results obtained from the MD simulations. With this end in mind, Figure 4 shows the joint probability distribution of angles α and β (upper panels) and ϵ and ζ (lower panels) as obtained for trajectory MD1 and for the additional MD run at 350 K. While at 300 K all four backbone angles are well described by a single mean value, the enhanced sampling calculation at 350 K reveals that several conformations may be accessible. Also shown are the values (as red dots) of the backbone angles α, β, ϵ, and ζ that are consistent with the analysis of the experimental data, as well as the values (as asterisks) of the canonical A and B forms. Moreover, for easy comparison, the experimental and calculated results for all backbone dihedral angles are comprised in Table 1.

Taking all possible experimental and calculated values shown into consideration, we find a good overall agreement of NMR and simulation. This agreement, however, is not always obtained for the values originally assigned from the experimental analysis. Considering again the U7 nucleotide as a representative example, we find that angle β is well reproduced for all nucleo-

Table 1. Comparison of Experimental and Calculated Backbone Dihedral Angles, in Degrees, of the UUUU Loop

	U4	U5	U6	U7
α^{NMR}	−75, −150, 0, 100	−120, 52	–	−120, 29, 75
$\alpha^{MD1,350K}$	−73, −133	−70, −132	−71, −154	−87, −109
β^{NMR}	−174 (1)	−184 (1)	180 (50)	−165 (2)
$\beta^{MD1,350K}$	−187, −180	−188, −177	173, 154	−175, −173
γ^{NMR}	57	68	–	53
$\gamma^{MD1,350K}$	63, 117	72, 122	183, 120	58, 91
δ^{NMR}	67	110	113	118
$\delta^{MD1,350K}$	80, 87	143, 117	75, 102	138, 136
ϵ^{NMR}	−235 (2), −146 (1)	−231 (2), −145 (2)	−235 (1), −125 (2)	−237(1), −120 (2)
$\epsilon^{MD1,350K}$	−166, −150	−268, −115	−176, −153	−260, −193
ζ^{NMR}	−245, −100, 80	−125, −170, 50	−105, −70, 80	−185 −225, 25, 45, 55
$\zeta^{MD1,350K}$	−54, −79	−286, −184	63, 125	49, −268

The NMR data for angles α, β, ϵ, and ζ are the values that are consistent with the analysis in Figure 3; the rmsd of the fit of β and ϵ is given in parenthesis. The calculated data are the mean values of the angles obtained from trajectory MD1 and the enhanced sampling simulation at 350 K.

tides, since it is well described by a single value in calculation and experiment. This is in contrast to the findings for angle α, for which the enhanced sampling calculation suggests that several—typically two—regions of α are thermally populated. As a consequence, two experimental values, $\alpha = -120°$ and 75°, are consistent with the MD data. A clear change of the original data analysis is found for angles ϵ and ζ, since the MD calculations seem to clearly outrule the originally adopted value of $\epsilon = -237°$. Assuming $\epsilon = -120°$, we obtain a reasonable agreement for angle ζ for the nucleotides U4, U5, and U7, whereas the situation is still not clear for U6. Summing up the results shown in Figure 4 and Table 1, it has been shown that independently performed, unrestrained MD simulations may significantly clarify the analysis of conformationally averaged NMR.

While the MD structures are directly obtained from the trajectories, the experimental structures are calculated from various NMR data by additionally employing theoretical models such as Karplus relations. To investigate the validity and the accuracy of the latter, it is instructive to reverse this procedure by employing the models to calculate NMR observables from the MD trajectory. As an example, Figure 5 compares various ^3J couplings as obtained from NMR and MD. Let us first consider the couplings $^3J(H5'^{proS/R},P)$ and $^3J(C4'_i,P_i)$, which reflect angle β. Consistent with the perfect agreement of the experimental and calculated values for β in Figure 4, the calculated couplings $^3J(H5'^{proS/R},P)$ match the NMR data well. Surprisingly, however, the NMR and MD results obtained for $^3J(C4'_i,P_i)$ differ significantly, which suggests that the Karplus relation Equation 2 may not be appropriate in this case. In order to study whether insufficient sampling might be the origin of these deviations, Figure 5 also displays the corresponding results for the 350 K and the locally enhanced sampling (LES, see Experimental Procedures) trajectory. Generally speaking, the results for both enhanced sampling trajectories are quite similar to each other, but they are not necessarily better than the results of trajectory MD1. This finding indicates that, although improved sampling is clearly necessary, there are also deficiencies of the force field used in the MD simulations.

As a second example, we consider the couplings $^3J(H3',P)$, $^3J(C2',P)$, and $^3J(C4'_i,P_{i+1})$, which reflect the ϵ. While experimental and calculated ^3J couplings and ϵ perfectly agree for U4, the comparison is less consistent for the remaining residues. According to the couplings $^3J(H3',P)$ and $^3J(C4'_i,P_{i+1})$, for example, the values of ϵ for U7 obtained from NMR and MD1 should match well; however, this is not the case. The discrepancy is also not removed by improving the sampling, which suggests that either the force field or the Karplus relation (or both) causes the problem. In the case of U6, on the other hand, enhanced sampling leads to a significant improvement of the ^3J couplings. This result clearly reflects the large flexibility of the U6 residue, the appropriate description of which requires advanced sampling techniques.

Sugar Conformations

Information on the state of the sugar puckers can be obtained from the couplings $^3J(H1',H2')$, $^3J(H2',H3')$, and $^3J(H3',H4')$ shown in Figure 5. Except for residue U6, the couplings obtained from trajectory MD1 are seen to reproduce the NMR data well. On the other hand, trajectory MD2 again shows qualitative deviations from the experimental data. The fact that the NMR values for the U6 couplings lie in between the calculated values for MD1 and MD2 indicates insufficient sampling for the U6 residue. Indeed, the results for the U6 couplings of the 350 K and LES trajectories nicely match the experimental data, while the corresponding results for the U5 couplings deteriorate. The latter finding is a consequence of the fact that the 350 K trajectory also shows significant conformational heterogeneity of the U5 residue (see Figure 2), which is not observed experimentally.

The sugar conformations of the UUUU loop have also been determined by dipole-dipole crosscorrelated relaxation measurements (Felli et al., 1999). Figure 6 shows the relaxation rates $\Gamma^c_{C1H1,C2H2}$ and $\Gamma^c_{C3H3,C4H4}$ as obtained from NMR and various MD runs (see Equation 4). Again, trajectory MD1 is in better agreement with experimental data than trajectory MD2. Improving the sampling leads to a significantly better agreement for the 350 K trajectory, particularly for the U6 residue. Also shown in Figure 6 is the ratio of the two rates, which to

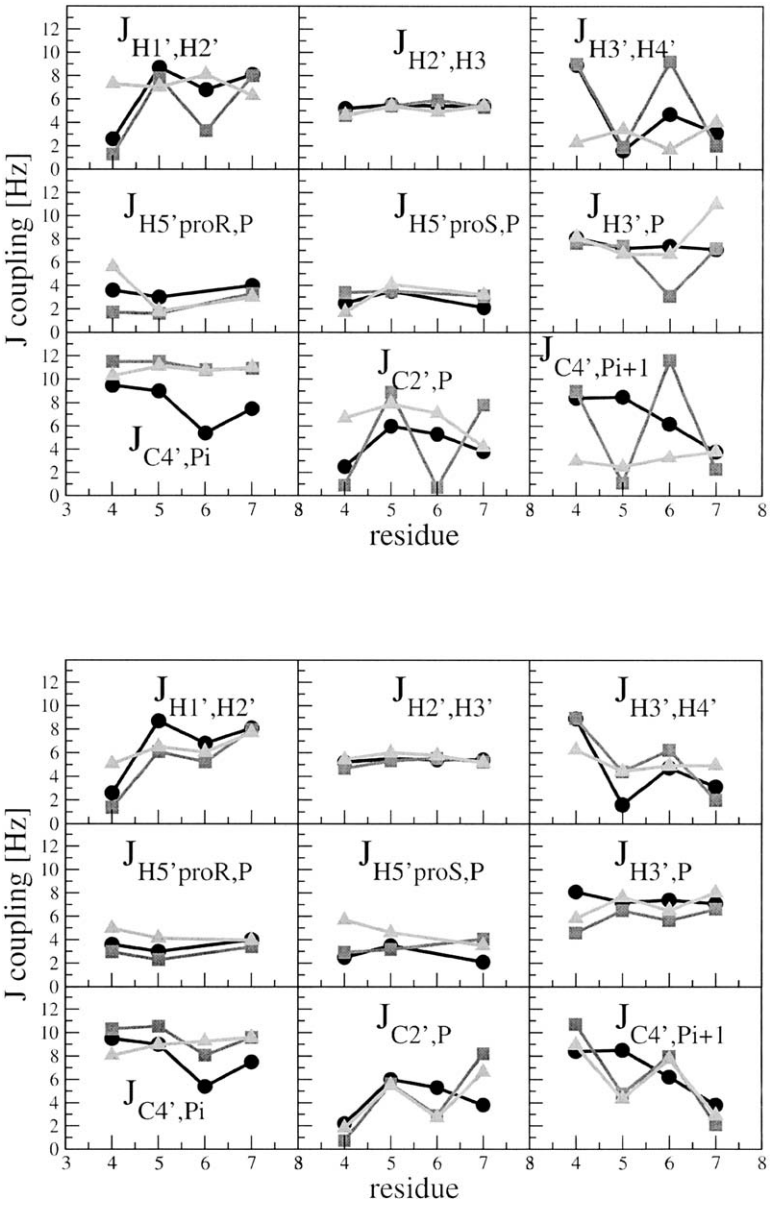

Figure 5. Experimental and Simulated ^3J Couplings of the UUUU Loop

Upper panel: comparison of the two 300 K trajectories MD1 (squares) and MD2 (triangles) to NMR data (dots). Lower panel: comparison of the 350 K trajectory (squares) and the LES trajectory (triangles) to NMR data (dots).

some extent eliminates the effects of the assumed overall correlation time τ_c and order parameters S^c_{ij}. Interestingly, the ratios are reproduced much better by the calculations than the individual rates. In particular, the results for trajectory MD1 are in excellent agreement with experimental data. As discussed in the original NMR report (Felli et al., 1999), the individual crosscorrelated relaxation rates are influenced by conformational dynamics (presumably of the sugar pucker) and can therefore not be fitted by a single overall correlation time τ_c and the order parameter $S^c_{ij} = 1$. However, τ_c and S^c_{ij} should be the same for each individual sugar, since the motion within one ribosyl moiety is correlated. In this case, the ratio $\Gamma^c_{C1H1,C2H2}/\Gamma^c_{C3H3,C4H4}$ of the cross-correlated relaxation rates does not depend on the assumption of overall τ_c and S^c_{ij}. Dropping the assumption, the MD simulations are in good agreement with the experimental data.

NOE Distances

For the UUUU loop, a total of 79 NOEs have been measured. For all intranucleotide NOEs as well as for NOEs associated with base-paired nucleotides, we have found excellent agreement between the distances obtained from experimental data and all MD calculations (data not shown). The remaining nine structural (i.e., internucleotide but not base-paired) NOEs are listed in Table 2. The results for trajectories MD1 and for the 350 K run are in good overall agreement with experimental data and show only one prominent deviation, U5-H3′;U6-H6. The agreement of NMR and trajectory MD2 is only slightly worse, with two nonmatching NOEs, C3-H3′;U4-H6 and U4-H2′;U5-H6. The LES simulation differs in all three mentioned NOEs from the NMR data. It is noted that in virtually all cases, the calculated NOE distances are larger than the experimentally measured ones. This finding indicates some confor-

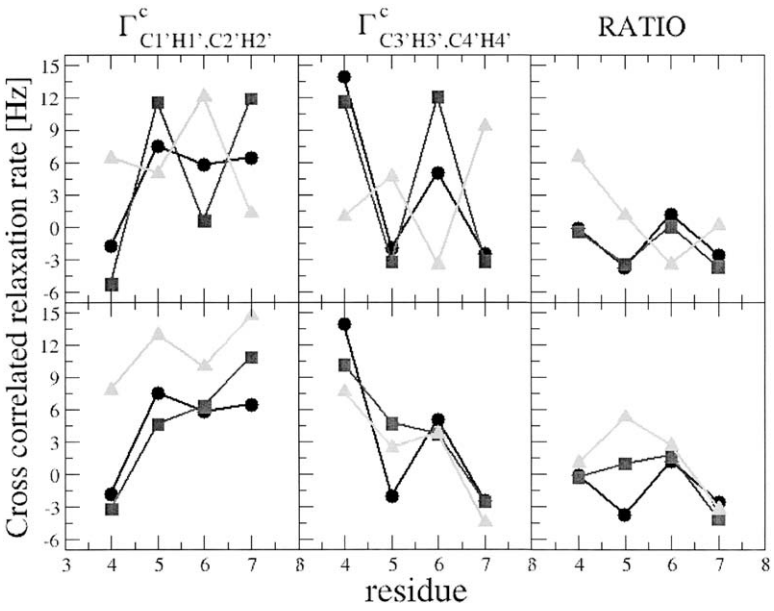

Figure 6. Experimental and Simulated Dipole-Dipole Crosscorrelated Relaxation Rates of the UUUU Loop

Upper panel: comparison of the two 300 K trajectories MD1 (squares) and MD2 (triangles) to NMR data (dots). Lower panel: comparison of the 350 K trajectory (squares) and the LES trajectory (triangles) to NMR data (dots).

mational heterogeneity, where conformations with larger distances are suppressed in the $\langle r^{-6} \rangle$ averaging process of the NOE measurement (Neuhaus and Williams, 2000).

Conformational Dynamics

Although trajectory MD1 is in good overall agreement with the NMR data, the above-mentioned results have shown that improved sampling strategies such as LES or high-temperature simulations are necessary to catch the experimentally observed transitions of the U6 sugar ring. Moreover, Figure 4 revealed that these simulations exhibit conformational heterogeneity with respect to the backbone dihedral angles α and χ. This finding indicates the possibility of further conformational transitions of the UUUU loop. In the following paragraphs, we describe how we adopted the 350 K trajectory to investigate the nature of these conformational dynamics in some detail. The reason that we prefer the high-temperature run over the LES simulation is two fold. The analysis, as well as the interpretation, of a standard MD trajectory is more straightforward, and the overall results are in better agreement with a recently performed replica exchange MD simulation of the UUUU loop (J.K. et al., unpublished data).

To identify and characterize the various conformations adopted by the 350 K simulation, we have performed a principal component analysis (PCA) of all atoms of the UUUU loop (see Experimental Procedures). Figure 7A shows the resulting free energy surface as a function of the first two principal components. The free energy landscape exhibits several minima, labeled by the numbers 1–4. To clearly separate minima 3 and 4, it is necessary to invoke a third principal component (data not shown). The population probabilities of the four states are 14%, 20%, 40%, and 17%, which correspond to free energy differences of less than 1 kcal/mol. The minima of free energy correspond to various conformational structures displayed in Figure 8. The four structures found in the simulation are seen to differ mainly in the stacking interactions of their bases: structure 1 exhibits a stacking of the bases of residues U4 and U5; it essentially reflects the average structure found in trajectory MD1. Structures 2 and 3 represent the most populated conformations of the loop. Both structures show a stacking of the bases U5 and U7, but they differ in the position of the U6 residue: in structure 2, U6 points into the solvent (as in structure 1); in structure 3, U6 is close (but not stacking) to U7. Finally, structure 4 exhibits a stacking of the bases of residues U6 and U7. All structures show a stable stacking interaction between the bases of the loop residue U4 and the stem residue C3.

The initial NMR structure that was used as starting

Table 2. Comparison of Calculated and Experimental NOEs, in Å, of the UUUU Loop

NOE	MD1	MD2	LES	350 K	NMR
C3-H6;U2-H2′	4.1 ± 0.4	4.1 ± 0.4	3.8 ± 0.3	4.2 ± 0.5	2.0 ± 0.5
C3-H6;U2-H3′	4.0 ± 0.4	3.4 ± 0.4	3.5 ± 0.3	3.6 ± 0.5	4.0 ± 1.0
G2-H1;G8-H1	3.9 ± 0.4	3.4 ± 0.3	3.7 ± 0.4	3.6 ± 0.4	4.5 ± 1.0
G10-H1;G2-H1	4.5 ± 0.6	4.2 ± 0.5	4.4 ± 0.5	4.9 ± 0.9	4.0 ± 1.0
U4-H6;C3-H3′	3.0 ± 0.3	7.9 ± 0.4	6.7 ± 1.2	3.6 ± 0.7	3.0 ± 0.5
U5-H6;U4-H2′	3.6 ± 0.4	11.1 ± 1.0	7.0 ± 1.4	5.8 ± 1.0	3.0 ± 0.5
U6-H6;U5-H3′	7.8 ± 0.8	4.7 ± 2.3	8.4 ± 1.4	8.7 ± 1.3	4.0 ± 1.0
G8-H8;U7-H1′	4.0 ± 0.8	4.8 ± 1.1	3.9 ± 0.8	4.0 ± 1.5	3.0 ± 0.5
C9-H6;G8-H3′	3.9 ± 0.5	4.1 ± 0.4	3.3 ± 0.3	3.6 ± 0.5	2.0 ± 0.5

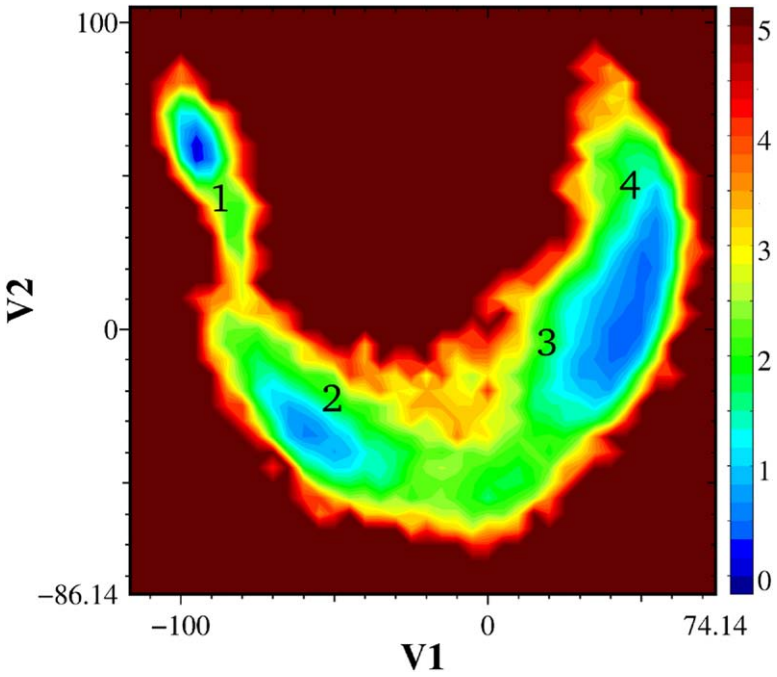

Figure 7. Free Energy Surface, in Units of kcal/mol, Obtained from the MD Simulation at 350 K, Plotted as a Function of the First Two Principal Components

geometry for the simulation is qualitatively similar to structure 1. Interestingly, however, no NOEs revealing intensive base stacking could be observed, not even between the U4 and C3 bases. However, some experimental evidence on stacking interactions is provided by the H6 chemical shifts (U7: δ = 7.81 ppm; U5: δ = 7.71 ppm; U4: δ = 7.68 ppm; U6: δ = 7.52 ppm) (Richter, 1999). These data show that U7 provides the most downfield proton reflecting some stacking, while U6 provides the most shielded proton, presumably due to the lack of any stacking interactions (Cromsigt et al., 2001). It should be noted that there is also very little

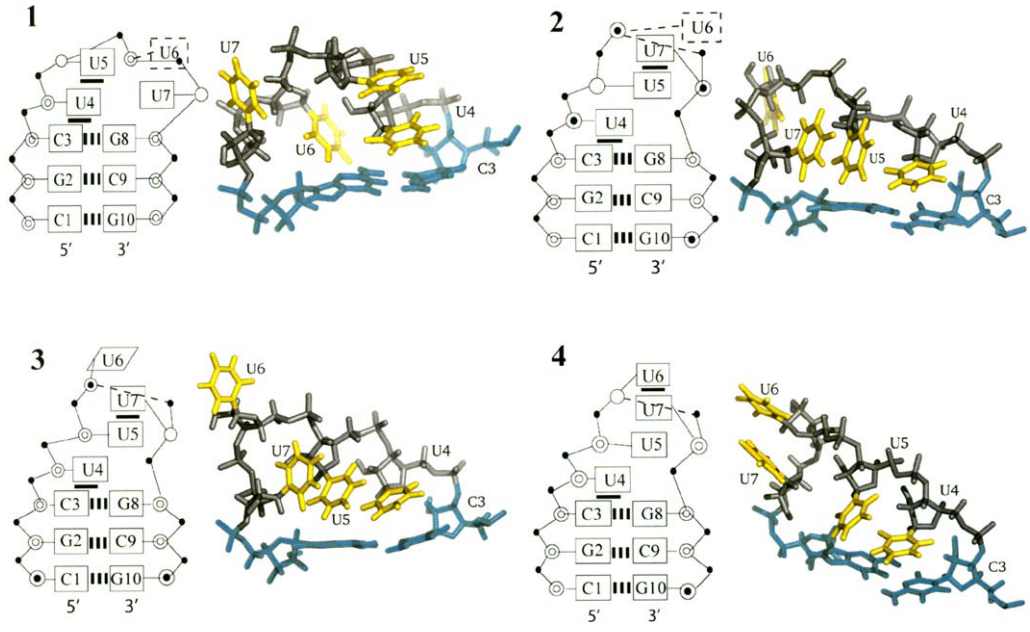

Figure 8. Conformations from MD Simulations of the UUUU Tetraloop at 350 K

(Left) Illustration of the four conformational states of the UUUU loop found in the MD simulation at 350 K. Dashed lines indicate that the residue points into the solvent. The symbols denote closed circle, phosphate; parallel lines, Watson-Crick pairings; thick dash, stacking interaction; open circle, C2′-endo ribose; bullseye, C3′-endo ribose; and circle with dot in the middle, C2′- and C3′-endo ribose.
(Right) MD snapshots of the loop structures obtained for the conformational states.

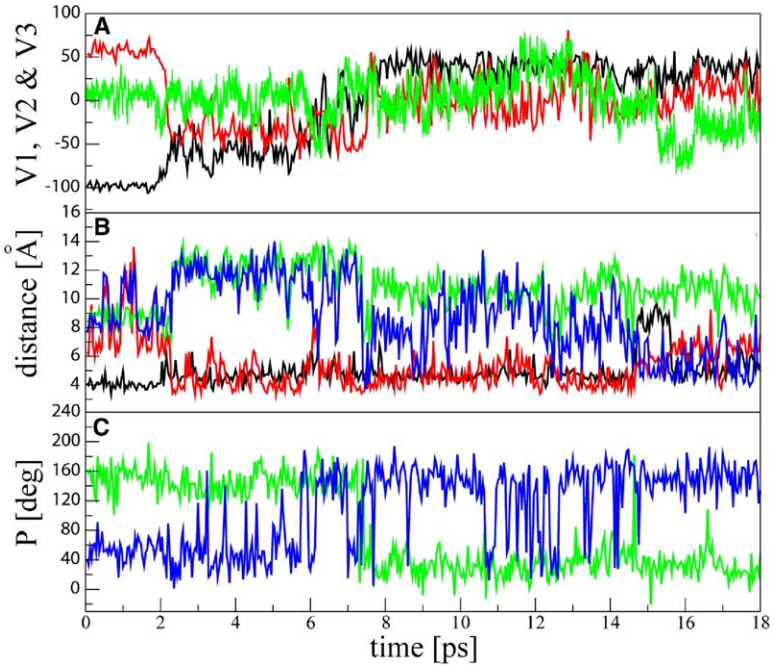

Figure 9. Conformational Dynamics of the UUUU Loop as Observed in the Time Evolution of the MD Trajectory at 350 K

(A) Projection of the trajectory on its first (black), second (red), and third (green) principal component, respectively.

(B) Distances between the loop nucleotides U4 and U5 (black), U5 and U7 (red), U5 and U6 (green), and U6 and U7 (blue).

(C) Pseudorotation angles of residues U5 (blue) and U6 (green).

stacking observed for trajectory MD2, which has two residues (U5 and U6) pointing into the solvent. However, the structure of trajectory MD2 was hardly sampled in the 350 K and the LES simulations, which may also explain the unsatisfactory agreement of this trajectory with experimental data.

To reveal the underlying dynamics of this conformational heterogeneity, Figure 9 shows the time evolution of the projection of the MD trajectory on the first two principal components (Figure 9A) and the stacking interactions of base pairs U4-U5, U5-U6, U5-U7, and U6-U7 (Figure 9B) as monitored by the distances between their centers of mass. Considering a distance $<\sim 5$ Å as indicative for base stacking, it is found that the bases U4 and U5 are stacked throughout the trajectory, the bases U5 and U7 are stacked during 2 ns $< t <\sim 15$ ns, the bases U6 and U7 are stacked for $t >\sim 15$ ns, and the bases U5 and U6 are not stacked at all. As anticipated in the discussion of the PCA energy surface and the corresponding conformational structures of the UUUU tetraloop, there is a clear correlation between the dynamics of the principal components shown in (Figure 9A) and the dynamics of the base distances in shown (Figure 9B). The time evolution of these quantities can be roughly divided up into four periods: (1) 0–2.5 ns, (2) 2.5–6 ns, (3) 8–15 ns, and (4) 15–18 ns, which are found to directly correspond to the free energy minima and structures shown in Figures 7 and 8, respectively. Moreover, the conformational rearrangement from structure 2 to structure 3 during times 6–8 ns is reflected in a shallow low-energy region between the free energy minima 2 and 3 in Figure 7. Hence, the time evolution of the base distances accounts almost completely for the main conformational dynamics described by the first few principal components.

Figure 9C also shows the time evolution of the pseudorotation angle P of the sugar rings U5 and U6. The data for the U6 angle nicely reproduce the experimental finding that the U6 sugar pucker is to 60% in the C2′-endo state (corresponding to P $\approx$ 150°) and to 40% in the C3′-endo state (corresponding to P $\approx$ 20°). As discussed above, the 350 K simulation also predicts significant conformational heterogeneity of the U5 sugar ring, which does not match the experimental result that the U5 sugar pucker is to 90% in the C2′-endo state. Moreover, the calculated time evolution of the remaining two pseudorotational angles (data not shown) predicts the C3′-endo state for the U4 sugar and the C2′-endo state for the U7 sugar, which again are in good agreement with experimental data.

Most interestingly, however, Figure 9 clearly shows that there is no correlation between the dynamics of the sugar rings and the stacking dynamics of the loop bases. We have also considered the time evolution of the torsional angles χ, which describe the relative orientation of the sugar ring and the base. Throughout the simulation, we could find very little correlation of the χ angles with the dynamics of the sugar rings or the stacking of the bases (data not shown). This finding is somewhat surprising because of the well-known fact that the A and B forms of DNA and RNA are clearly correlated with the conformation of the sugar rings, i.e., the C3′-endo state for the A forms and the C2′-endo state for the B forms.

Discussion

We have presented a comprehensive NMR/MD study of the structure and dynamics of the UUUU tetraloop. As a first goal of the paper, we have studied the performance of the theoretical model, that is, the quality of the force field and the conformational sampling achieved. As a second goal, we have employed both

experimental and theoretical data to draw a dynamic picture of the RNA hairpin.

Concerning the sampling achieved in the MD simulations, it has been shown that a conventional room-temperature MD run on a 10 ns timescale cannot account for the conformational heterogeneity of a flexible RNA tetraloop. This is clearly demonstrated by the calculations of the ^{3}J couplings of the U6 residues in Figure 5, in which the results of 300 K runs MD1 and MD2 are shown to be either too high or too low compared to experimental data, while both enhanced-sampling simulations yield average values close to experimental data. Moreover, the time traces of the 350 K and the LES simulation indicate that even these enhanced-sampling methods do not yield converged data for the UUUU tetraloop on a 10 ns timescale. Nonetheless, the overall results of the 350 K simulation are in good agreement with the 300 K data of a recently performed replica exchange MD simulation of the UUUU tetraloop (J.K. et al., unpublished data), and they therefore appear to draw a realistic picture of the conformational heterogeneity of the RNA tetraloop.

Concerning the quality of the force field, we have found that the 300 K trajectory MD1 is in surprisingly good overall agreement with experimental data, despite its insufficient sampling. The simulation yields only a single nonmatching NOE and—with the exception of the undersampled U6 residue—^{3}J couplings and dipole-dipole crosscorrelated relaxation rates that reproduce the NMR data well in most cases. The overall good agreement is also reflected in the fact that trajectory MD1 is able to perfectly recover the first four backbone dihedral angles α, β, γ, and δ, while there are some deviations for angles ϵ and ζ. Enhancing the sampling in the 350 K and LES simulations, the results for the U6 residue improve as expected, while the corresponding results for the U5 residue deteriorate, since the U5 sugar ring is too flexible compared to experimental data. Nonetheless, considering the unusual amount of experimental results that are available for the UUUU tetraloop, it seems fair to say that the AMBER98 force field does a surprisingly good job at reproducing the NMR data.

To characterize the structure and the conformational heterogeneity of the UUUU tetraloop, we have performed a principal component analysis of the 350 K trajectory. The resulting free energy surface exhibits four minima that correspond to well-defined conformational structures, which differ mainly by their base stacking in the loop region. Interestingly, the NMR structure used as a starting condition for the MD simulation did not show any of these stacking interactions. By following the time evolution of various quantities such as principal components, base distances, and sugar pseudorotation angles (see Figure 9), we have found no correlation between the motion of the sugar rings and the stacking dynamics of the loop bases. This finding is somewhat surprising because of the well-known fact that the A and B forms of DNA and RNA are clearly correlated with the conformation of the sugar rings, i.e., the C3′-endo state for the A forms and the C2′-endo state for the B forms.

It is tempting to speculate that the conformational flexibility of the UUUU loop is necessary for its function. In the case of the hammerhead ribozyme, recent data of Persson et al. (2002) support the idea that the increased flexibility of the UUUU tetraloop compared to the more stable GNRA tetraloop may allow increased sampling of those conformations of the ribozyme that are catalytically more active. It is noted, however, that the difference in the melting free energy between the seemingly rigid tetraloop architecture of GNRA and for the substantially dynamic UUUU tetraloop is surprisingly small ($\Delta\Delta G \approx 1$kcal/mol) (Persson et al., 2002). This is because the conformational heterogeneity results in a larger entropic gain upon melting, although the enthalpic contribution is smaller for a flexible system. As a consequence, the conformational heterogeneity of the RNA hairpin with its various, almost isoenergetic, stacking arrangements does not necessarily affect the overall stability of the system. NMR and MD appear as a promising combination to shed light on this subtle interplay between dynamics and stability.

Experimental Procedures

MD Simulations

All simulations were performed by using the AMBER6 simulation program package (Case et al., 1999) employing the all-atom force field parm98 (Cheatham et al., 1999). The UUUU tetraloop consists of 314 atoms that were placed in a periodic truncated octahedral box of TIP3P water (Jorgensen et al., 1983). Including 9 Na^+ ions to neutralize the system, a total of 7709 atoms are obtained. The equation of motion was integrated by using a leapfrog algorithm with a time step of 2 fs. The SHAKE algorithm (Ryckaert et al., 1977) was used to constrain covalent bonds to hydrogen atoms with a relative geometric tolerance of 10^{-4}. A cutoff of 10 Å was chosen for the nonbonded van der Waals interactions. We used the particle-mesh Ewald method (Darden et al., 1993) to treat the long-range electrostatic interactions and updated the nonbonded interaction pair-list every 10 fs. The solute and solvent were separately weakly coupled to external temperature baths at 300 K (Berendsen et al., 1984), by using a coupling constant of 0.2 ps. The total system was also weakly coupled to an external pressure bath at 1 atm by using a coupling constant of 0.5 ps.

From about 100 available NMR structures of the UUUU loop, 4 representative MD starting structures were selected by using the clustering program NMRCLUST (Kelley et al., 1996). For each structure, the equilibration protocol consisted of 200 steps of steepest-descent minimization applied to the solvent molecules with fixed solute, followed by 100 ps of MD simulation of the solvent with the fixed tetraloop, and another 500 ps of simulation without positional constraint of the tetraloop. During the subsequent unrestrained MD runs, two of the four NMR structures showed base pair disruption after 0.5 and 3 ns, respectively. The simulations for the remaining two NMR structures, referred to as MD1 and MD2, were continued for another 12 ns, and the coordinates were saved every 1 ps for analysis.

To improve the conformational sampling obtained in the MD simulations, two strategies were employed. First, we performed a 18 ns high-temperature MD run at 350 K, using the final structure of trajectory MD1 as starting geometry. Furthermore, the locally enhanced sampling (LES) method (Elber and Karplus, 1990; Simmerling et al., 1998), as implemented in the AMBER6 program package, was employed. In order to focus the computational effort on the part of the system that is of interest, in the present case the flexible loop region, the LES method replaces the trajectory of this part by an ensemble of copies, which interact with the remaining system through an average over the copies. This mean field description results in a smoothing of the energy landscape by a lowering of the barriers, thus improving the conformational sampling of the subsystem of interest. Following the work done by Simmerling et al. (1998), we performed a 4 ns LES simulation with five copies of the loop region.

Calculation of NMR Data

To calculate the ^3J couplings shown in Figure 5, the following Karplus relations (in units of Hz) were employed (Wijmenga and Van Buuren, 1998):

$$^3J(H,P) = 15.3\cos^2\phi - 6.2\cos\phi + 1.5, \quad (1)$$

$$^3J(C,P) = 6.9\cos^2\phi - 3.4\cos\phi + 0.7, \quad (2)$$

$$^3J(H,H) = 13.24\cos^2\phi - 0.91\cos\phi + \sum_{i=1}^{4}\Delta\chi_i \{0.53 - 2.41\cos^2(\zeta_i\phi + 15.5|\Delta\chi_i|)\}. \quad (3)$$

Equation 1 was used to calculate the couplings $^3J(H5'^{proS,R},P)$ (ϕ = $\beta \pm 120°$) and $^3J(H3',P)$ ($\phi = \epsilon + 120°$), Equation 2 was used to calculate the couplings $^3J(C4'_i,P_i)$ ($\phi = \beta$), $^3J(C2'_i,P_{i+1})$ ($\phi = \epsilon - 120°$), and $^3J(C4'_i,P_{i+1})$ ($\phi = \epsilon$), and Equation 3 was used to calculate the couplings $^3J(H1',H2')$, $^3J(H2',H3')$, and $^3J(H3',H4')$, where ϕ is a function of the pseudorotation angle P of the sugar pucker; the parameters $\Delta\chi_i$ and ζ_i for the hydrogen pairs of the sugar ring are given in Wijmenga and Van Buuren (1998). In all cases, the ^3J couplings were obtained by averaging Equations 1–3 over all angles sampled by the MD trajectory.

To calculate the crosscorrelated relaxation rate $\Gamma^C_{C_iH_i,C_jH_j}$ between the dipolar interactions of two distinct carbon-proton spin pairs (C_i, H_i) and (C_j, H_j), we employed the expression (Felli et al., 1999)

$$\Gamma^C_{C_iH_i,C_jH_j} = \frac{2}{5}\frac{\gamma_H^2\gamma_C^2}{r^3_{C_iH_i}r^3_{C_jH_j}}\left(\frac{\mu_0}{4\pi}\right)^2\hbar^2(S^c_{i,j})^2\left(\frac{3\cos^2\theta_{ij}-1}{2}\right)\tau_c, \quad (4)$$

where γ_C and γ_H are the gyromagnetic ratios, μ_0 is the susceptibility of vacuum, $r_{Ci\ Hi}$ and $r_{Cj\ Hj}$ are the carbon-proton distances, τ_c is the overall correlation time, (S^c_{ij}) is an order parameter accounting for the internal mobility of the dipole tensors of C_iH_i and C_jH_j, and θ_{ij} is the projection angle between these dipole tensors, which are oriented parallel to the respective carbon-proton bond vectors. In the calculations reported below, we have assumed rigid C-H vectors, which results in $S^c_{ij} = 1$. Furthermore, we choose τ_c = 1.8 ns, as determined by experimental data. From the MD simulation, the bond distances r_{CiHi} and r_{CjHj} as well as the projection angle θ_{ij} are obtained.

Principal Component Analysis

To identify the most important conformational degrees of freedom of a simulation, the PCA method, also called quasiharmonic analysis or the essential dynamics method, has been proven useful (Amadei et al., 1993; Becker, 1997; Garcia, 1992; Hayward et al., 1993; Ichiye and Karplus, 1991). The approach is based on the covariance matrix

$$\sigma_{ij} = \langle(x_i - \langle x_i\rangle)(x_j - \langle x_j\rangle)\rangle, \quad (5)$$

where x_1, ... x_{3N} are the mass-weighted Cartesian coordinates of the N-particle system, and <…> denotes the average over all sampled conformations. Since the covariance matrix provides information on the correlated fluctuations of pairs of atoms, its eigenvectors and eigenvalues of σ yield the modes of collective motion and their amplitudes. To remove the overall rotation of the trajectory, its initial geometry was chosen as a reference structure for the rotational fit. Because the UUUU tetraloop does not undergo major large-amplitude motion, the results of the PCA are quite insensitive to the choice of the reference structure.

Since we wish to focus on the conformation dynamics of the loop region, the PCA was restricted to the atoms of the four loop residues. By diagonalizing the resulting covariance matrix, we obtain the eigenvectors v_n and the eigenvalues λ_n, which are organized in descending order, i.e., λ_1 represents the largest eigenvalue. In the PCA of the loop region, the motions along the first two eigenvectors, v_1, v_2 of σ, contain 70% of the fluctuations of the 350 K simulation. Restricting ourselves to these first two eigenvectors, the free energy surface along these vectors is given by

$$\Delta G(v_1, v_2) = -k_BT[\ln P(v_1, v_2) - \ln P_{max}]. \quad (6)$$

Here $P(v_1,v_2)$ is the probability distribution obtained from a histogram of the MD data and P_{max} denotes the maximum of the distribution, which is subtracted to ensure that $\Delta G = 0$ for the lowest free energy minimum. The representation of the free energy surface as a function of higher eigenvectors was found to not yield significantly more information, apart from the fact that structures 3 and 4 in Figure 8 can be distinguished more clearly.

Acknowledgments

We thank Phuong Nguyen and Jens Wöhnert for numerous inspiring and helpful discussions. This work has been supported by the Deutsche Forschungsgemeinschaft through the Sonderforschungsbereich 579 "RNA-ligand interactions," by the Frankfurt Center of Scientific Computing, and by the state of Hesse for support of the Center for Biomolecular Magnetic Resonance.

Received: February 20, 2005
Revised: March 31, 2005
Accepted: May 13, 2005
Published: September 13, 2005

References

Amadei, A., Linssen, A.B., and Berendsen, H.J. (1993). Essential dynamics of proteins. Proteins *17*, 412–425.

Antao, V.P., Lai, S.Y., and Tinoco, I., Jr. (1991). A thermodynamic study of unusually stable RNA and DNA hairpins. Nucleic Acids Res. *19*, 5901–5905.

Auffinger, P., and Westhof, E. (2000). RNA solvation: a molecular dynamics simulation perspective. Biopolymers *56*, 266–274.

Auffinger, P., Bielecki, L., and Westhof, E. (2003). The Mg^{2+} binding sites of the 5S rRNA loop E motif as investigated by molecular dynamics simulations. Chem. Biol. *10*, 551–561.

Becker, O.M. (1997). Geometric versus topological clustering: an insight into conformation mapping. Proteins *27*, 213–226.

Berendsen, H., Postma, J., and Gunsteren, W.V. (1984). Molecular dynamics with couplings to an external bath. J. Chem. Phys. *81*, 3684–3690.

Beveridge, D.L., and McConnell, K.J. (2000). Nucleic acids: theory and computer simulation, Y2K. Curr. Opin. Struct. Biol. *10*, 182–196.

Butcher, S.E., Dieckmann, T., and Feigon, J. (1997). Solution structure of a GAAA tetraloop receptor RNA. EMBO J. *16*, 7490–7499.

Case, D.A., Pearlman, D.A., Caldwell, J.W., Cheatham, T.E., III, Ross, W.S., Simmer-ling, C.L., Darden, T.A., and Merz, J.K.M., Stanton, R.V., Cheng, A.L., et al. (1999). AMBER 6 (computer program). University of California.

Cheatham, T.E., III. (2004). Simulation and modeling of nucleic acid structure, dynamics and interaction. Curr. Opin. Struct. Biol. *14*, 360–367.

Cheatham, T.E., III, Cieplak, P., and Kollman, P.A. (1999). A modified version of the Cornell et al. force field with improved sugar pucker phases and helical repeat. J. Biomol. Struct. Dyn. *16*, 845–862.

Cheong, C., Varani, G., and Tinoco, I., Jr. (1990). Solution structure of an unusually stable RNA hairpin, 5′GGAC(UUCG)GUCC. Nature *346*, 680–682.

Conaty, J., Hendry, P., and Lockett, T. (1999). Selected classes of minimised hammerhead ribozyme have very high cleavage rates at low Mg^{2+} concentration. Nucleic Acids Res. *27*, 2400–2407.

Cromsigt, J.A., Hilbers, C.W., and Wijmenga, S.S. (2001). Prediction of proton chemical shifts in RNA. Their use in structure refinement and validation. J. Biomol. NMR *21*, 11–29.

Darden, T., York, D., and Petersen, L. (1993). Particle mesh ewald: An n·log(n) method for ewald sums in large systems. J. Chem. Phys. *98*, 10089–10091.

Du, Z., Yu, J., Andino, R., and James, T.L. (2003). Extending the family of UNCG-like tetraloop motifs: NMR structure of a CACG tetraloop from coxsackievirus B3. Biochemistry *42*, 4373–4383.

Duchardt, E., Richter, C., Reif, B., Glaser, S.J., Engels, J.W., Griesinger, C., and Schwalbe, H. (2001). Measurement of 2J(H,C)- and

3J(H,C)-coupling constants by alpha/beta selective HC(C)H-TOCSY. J. Biomol. NMR *21*, 117–126.

Durant, P.C., and Davis, D.R. (1999). Stabilization of the anticodon stem-loop of tRNALys,3 by an A+-C base-pair and by pseudouridine. J. Mol. Biol. *285*, 115–131.

Eckstein, F., Kore, A.R., and Nakamaye, K.L. (2001). In vitro selection of hammerhead ribozyme sequence variants. ChemBioChem *2*, 629–635.

Elber, R., and Karplus, M. (1990). Enhanced sampling in molecular dynamics: use of the time-dependent Hartree approximation for a simulation of carbon monoxide diffusion through myoglobin. J. Am. Chem. Soc. *112*, 9161–9175.

Felli, I.C., Richter, C., Griesinger, C., and Schwalbe, H. (1999). Determination of RNA Sugar pucker mode from cross-correlated relaxation in solution NMR spectroscopy. J. Am. Chem. Soc. *121*, 1956–1957.

Furtig, B., Richter, C., Bermel, W., and Schwalbe, H. (2004). New NMR experiments for RNA nucleobase resonance assignment and chemical shift analysis of an RNA UUCG tetraloop. J. Biomol. NMR *28*, 69–79.

Garcia, A.E. (1992). Large-amplitude nonlinear motions in proteins. Phys. Rev. Lett. *68*, 2696–2699.

Gouda, H., Kuntz, I.D., Case, D.A., and Kollman, P.A. (2003). Free energy calculations for theophylline binding to an RNA aptamer: comparison of MM-PBSA and thermodynamic integration methods. Biopolymers *68*, 16–34.

Hayward, S., Kitao, A., Hirata, F., and Go, N. (1993). Effect of solvent on collective motions in globular protein. J. Mol. Biol. *234*, 1207–1217.

Heus, H.A., and Pardi, A. (1991). Structural features that give rise to the unusual stability of RNA hairpins containing GNRA loops. Science *253*, 191–194.

Ichiye, T., and Karplus, M. (1991). Collective motions in proteins: a covariance analysis of atomic fluctuations in molecular dynamics and normal mode simulations. Proteins *11*, 205–217.

Jagath, J.R., Matassova, N.B., de Leeuw, E., Warnecke, J.M., Lentzen, G., Rodnina, M.V., Luirink, J., and Wintermeyer, W. (2001). Important role of the tetraloop region of 4.5S RNA in SRP binding to its receptor FtsY. RNA *7*, 293–301.

Jorgensen, W., Chandrasekhar, J., Madura, J., Impey, R., and Klein, M. (1983). Comparison of simple potential functions for simulating liquid water. J. Chem. Phys. *79*, 926–928.

Jucker, F., and Pardi, A. (1995). Solution structure of the CUUG hairpin loop: a novel RNA tetraloop motif. Biochemistry *34*, 14416–14427.

Jucker, F.M., Heus, H.A., Yip, P.F., Moors, E.H., and Pardi, A. (1996). A network of heterogeneous hydrogen bonds in GNRA tetraloops. J. Mol. Biol. *264*, 968–980.

Kajava, A., and Ruterjans, H. (1993). Molecular modelling of the 3-D structure of RNA tetraloops with different nucleotide sequences. Nucleic Acids Res. *21*, 4556–4562.

Kelley, L.A., Gardner, S.P., and Sutcliffe, M.J. (1996). An automated approach for clustering an ensemble of NMR-derived protein structures into conformationally related subfamilies. Protein Eng. *9*, 1063–1065.

Legault, P., Li, J., Mogridge, J., Kay, L.E., and Greenblatt, J. (1998). NMR structure of the bacteriophage lambda N peptide/boxB RNA complex: recognition of a GNRA fold by an arginine-rich motif. Cell *93*, 289–299.

Liu, H., Matsugami, A., Katahira, M., and Uesugi, S. (2002). A dimeric RNA quadruplex architecture comprised of two G:G(:A):G:G(:A) hexads, G:G:G:G tetrads and UUUU loops. J. Mol. Biol. *322*, 955–970.

Miller, J.L., and Kollman, P.A. (1997). Theoretical studies of an exceptionally stable RNA tetraloop: observation of convergence from an incorrect NMR structure to the correct one using unrestrained molecular dynamics. J. Mol. Biol. *270*, 436–450.

Neuhaus, D., and Williams, M.P. (2000). The Nuclear Overhauser Effect in Structural and Conformational Analysis (New York: Wiley-VCH).

Norberg, J., and Nilsson, L. (1995). Stacking free energy profiles for all 16 natural ribodinucleoside monophosphates in aqueous solution. J. Am. Chem. Soc. *117*, 10832–10840.

Norberg, J., and Nilsson, L. (2002). Molecular dynamics applied to nucleic acids. Acc. Chem. Res. *35*, 465–472.

Persson, T., Hartmann, R.K., and Eckstein, F. (2002). Selection of hammerhead ribozyme variants with low Mg^{2+} requirement: importance of stem-loop II. ChemBioChem *3*, 1066–1071.

Proctor, D.J., Schaak, J.E., Bevilacqua, J.M., Falzone, C.J., and Bevilacqua, P.C. (2002). Isolation and characterization of a family of stable RNA tetraloops with the motif YNMG that participate in tertiary interactions. Biochemistry *41*, 12062–12075.

Proctor, D.J., Ma, H., Kierzek, E., Kierzek, R., Gruebele, M., and Bevilacqua, P.C. (2004). Folding thermodynamics and kinetics of YNMG RNA hairpins: specific incorporation of 8-bromoguanosine leads to stabilization by enhancement of the folding rate. Biochemistry *43*, 14004–14014.

Richter, C. (1999). Entwicklung neuer NMR-Spektroskopischer Methoden zur Bestimmung der Konformation in Oligonukleotiden. Dissertation thesis, Johann Wolfgang Goethe-Universität, Frankfurt, Germany.

Richter, C., Reif, B., Worner, K., Quant, S., Marino, J.P., Engels, J.W., Griesinger, C., and Schwalbe, H. (1998). A new experiment for the measurement of nJ(C,P) coupling constants including 3J(C4′i,Pi) and 3J(C4′i,Pi+1) in oligonucleotides. J. Biomol. NMR *12*, 223–230.

Richter, C., Reif, B., Griesinger, C., and Schwalbe, H. (2000). NMR spectroscopic determination of angles alpha and zeta in RNA from CH-dipolar coupling, P-CSA cross-correlated relaxation. J. Am. Chem. Soc. *122*, 12728–12731.

Ryckaert, J.P., Ciotti, G., and Berensden, H.J.C. (1977). Numerical-integration of cartesian equations of motion of a system with constraints—molecular-dynamics of n-alkanes. J. Comput. Phys. *23*, 327–341.

Simmerling, C., Miller, J.L., and Kollman, P.A. (1998). Combined locally enhanced sampling and particle mesh ewald as a strategy to locate the experimental structure of a nonhelical nucleic acid. J. Am. Chem. Soc. *120*, 7149–7155.

Sorin, E.J., Engelhardt, M.A., Herschlag, D., and Pande, V.S. (2002). RNA simulations: probing hairpin unfolding and the dynamics of a GNRA tetraloop. J. Mol. Biol. *317*, 493–506.

Sorin, E.J., Rhee, Y.M., Nakatani, B.J., and Pande, V.S. (2003). Insights into nucleic acid conformational dynamics from massively parallel stochastic simulations. Biophys. J. *85*, 790–803.

Stuart, J.W., Gdaniec, Z., Guenther, R., Marszalek, M., Sochacka, E., Malkiewicz, A., and Agris, P.F. (2000). Functional anticodon architecture of human tRNALys3 includes disruption of intraloop hydrogen bonding by the naturally occurring amino acid modification, t6A. Biochemistry *39*, 13396–13404.

Tsui, V., and Case, D. (2001). Calculations of the absolute free energies of binding between RNA and metal ions using molecular dynamics simulations and continuum electrostatics. J. Phys. Chem. B *105*, 11314–11325.

Uhlenbeck, O.C. (1990). Tetraloops and RNA folding. Nature *346*, 613–614.

Wijmenga, S.S., and Van Buuren, B.N.M. (1998). The use of NMR methods for conformational studies of nucleic acids. Prog. Nucleic Magn. Reson. Spectrosc. *32*, 287–387.

Williams, D.J., and Hall, K.B. (1999). Unrestrained stochastic dynamics simulations of the UUCG tetraloop using an implicit solvation model. Biophys. J. *76*, 3192–3205.

Williams, D.J., and Hall, K.B. (2000a). Experimental and computational studies of the G[UUCG]C RNA tetraloop. J. Mol. Biol. *297*, 1045–1061.

Williams, D.J., and Hall, K.B. (2000b). Experimental and theoretical studies of the effects of deoxyribose substitutions on the stability of the UUCG tetraloop. J. Mol. Biol. *297*, 251–265.

Woese, C.R., Winker, S., and Gutell, R.R. (1990). Architecture of ribosomal RNA: constraints on the sequence of "tetra-loops." Proc. Natl. Acad. Sci. USA *87*, 8467–8471.

Wörner, K. (1997). Synthese und Charakterisierung kleiner strukturbildender Oligonukleotide. Dissertation thesis, Johann Wolfgang Goethe-Universität, Frankfurt, Germany.

Zacharias, M. (2000). Simulation of the structure and dynamics of nonhelical RNA motifs. Curr. Opin. Struct. Biol. *10*, 311–317.

Zacharias, M., and Sklenar, H. (1999). Conformational analysis of single-base bulges in A-form DNA and RNA using a hierarchical approach and energetic evaluation with a continuum solvent model. J. Mol. Biol. *289*, 261–275.